International Journal of Multiphase Flow 35 (2009) 914–923

Contents lists available at ScienceDirect

International Journal of Multiphase Flow

journal homepage: www.elsevier.com/locate/ijmulflow

Comparison of the RANS and PDF methods for air-particle flows

Alexander I. Kartushinsky [a,1], Efstathios E. Michaelides [b,*], Leonid I. Zaichik [c,2]

[a] Research Laboratory of Multiphase Media Physics, Tallinn University of Technology Akadeemia tee 21E, 12618 Tallinn, Estonia
[b] Mechanical Engineering, University of Texas AT San Antonio, San Antonio, TX 78258, USA
[c] Laboratory of Mathematical Modeling, Russian of Academy of Sciences, Institute for High Temperatures, Krasnokazarmennaya, 17a, 111250 Moscow, Russia

ARTICLE INFO

Article history:
Received 12 August 2008
Received in revised form 3 June 2009
Accepted 9 June 2009
Available online 13 June 2009

Keywords:
RANS
PDF
Models
Particulate flow
Pipe flow

ABSTRACT

Two simulation methods, namely Reynolds-Averaged Navier–Stokes (RANS) equations, and Probability Distribution Function (PDF) are currently widely used for the modeling of multiphase flows. These two approaches are supplemented with appropriate closure equations that take into account all the pertinent forces and interaction effects on the solid particles, such as: particle–turbulence interactions; turbulence modulation; particle–particle interactions; particle–wall interactions; gravitation, drag and lift forces. The two methods have been used in order to simulate the turbulent particulate flow in upward pipes. The flow domain in all cases was a cylindrical pipe and the computations were carried for upward pipe flow. Monodisperse as well as polydisperse mixtures of particles have been considered. In general, the average velocity results obtained from the two methods are in close agreement, because the methods predict well the average velocity distribution of the carrier fluid as well as the solids. Thus, the differences in the average axial velocities predicted by the methods are not substantial. Differences in the turbulence intensity are more significant. A comparison of the numerical results obtained shows the relative importance of retaining the diffusion terms in both the axial and radial directions in the RANS method. Also the comparisons of the results show the relative effect of the lift forces in the distribution of solid particles.

1. Introduction

The particulate flow in channels has numerous engineering applications ranging from pneumatic conveying systems to chemical reactor design and is one of the most thoroughly investigated subjects in the area of multiphase flow. Phenomenological models for particulate flows in pipes have been developed in the past, including those by Pfeffer et al. (1966) and Michaelides (1984). All studies show that turbulence plays a very important role in such flows, with the particles often modulating the turbulence structure of the carrier fluid (Elghobashi and Abou-Arab, 1983; Yarin and Hetsroni, 1994; Yuan and Michaelides, 1992; Crowe and Gillandt, 1998, etc.).

The multiphase flow modeling method, which is often called the "two-fluid model", has been applied successfully in the modeling of dispersed two-phase systems. In the two-fluid model, both the gas and particles are considered as two coexisting phases that span the entire flow domain, each flowing with its own mass fraction. In the case of polydisperse solid mixtures, each solids fraction is characterized by its own mass fraction. Momentum interactions between the two phases are characterized by drag force, which appears as source term in the numerical computations. Two different modeling methods for the description of the fluid and particle phase motion have been used in conjunction with the general approach of the two-fluid model:

- the Reynolds-Averaged Navier–Stokes equations (RANS) method;
- the Two-Phase Probability Distribution Function method.

The effects of these methods will be compared in this study, whose objectives are as follows:

(a) the development of appropriate numerical techniques for the implementation of the modeling methods;
(b) the generation of numerical results emanating from the two methods; and
(c) the comparison of the results of the two methods.

2. Model description for particulate flow in pipes

Without loss of generality, it is assumed that the solid phase is polydisperse and composed of particles of several sizes with known mass fractions, which are denoted by α_i. These fractions may be of single or different materials and are characterized by

* Corresponding author. Tel.: +1 210 458 5580.
E-mail addresses: aleksander.kartusinski@ttu.ee (A.I. Kartushinsky), Stathis.michaelides@utsa.edu (E.E. Michaelides), leonid.zaichik@mtu-net.ru (L.I. Zaichik).
[1] Tel.: +1 372 670 3610; fax: +1 372 670 3601.
[2] Tel.: +7 095 362 55 90; fax: +7 095 362 55 90.

0301-9322/$ - see front matter © 2009 Elsevier Ltd. All rights reserved.
doi:10.1016/j.ijmultiphaseflow.2009.06.002

their size and material density. For simplicity, in the formulation of the governing equations, three solid fractions, namely 1, 2 and 3, have been assumed to be present. Other numbers of fractions may be accounted for, by simply extending the upper limit in the pertinent summation operation. Hydrodynamic forces, such as drag and lift act on all particulate fractions. The complete sets of governing equations and boundary conditions for the two modeling methods are given in the following sub-sections:

2.1. Reynolds-Averaged Navier–Stokes (RANS) model

The RANS model is based on the solution of the complete Navier–Stokes equations, without using any simplifications as for example, the boundary layer assumptions that are inherent in the Turbulence Boundary Layer model. In this paper, the governing equations are written with the convective and diffusive terms on the left-hand side and the various interaction forces on the right-hand side of the corresponding equations.

2.1.1. Continuity for the gaseous phase

$$\frac{\partial u}{\partial x}+\frac{\partial (r v)}{r\partial r}=0, \tag{1}$$

where u and v are the axial and radial velocity components of the gas-phase, respectively and r is the radial coordinate.

2.1.2. Linear momentum equation in the longitudinal direction for the gaseous phase

$$\begin{aligned}&\frac{\partial}{\partial x}\left(u^2-\tilde{\nu}_t\frac{\partial u}{\partial x}\right)+\frac{\partial}{r\partial r}r\left(uv-\tilde{\nu}_t\frac{\partial u}{\partial r}\right)\\&\quad=-\frac{\partial p}{\rho\partial x}+\frac{\partial}{\partial x}\tilde{\nu}_t\frac{\partial u}{\partial x}+\frac{\partial}{r\partial r}r\tilde{\nu}_t\frac{\partial v}{\partial x}-\sum_{i=1,3}\alpha_i\left(\frac{u_{\mathrm{ri}}}{\tau_i'}+C_{\mathrm{Mi}}\Omega_i v_{\mathrm{ri}}\right),\end{aligned} \tag{2}$$

where $\tilde{\nu}_t=\nu_t+\nu$ is sum of the turbulent ν_t and laminar ν viscosities; p is the static pressure; α_i is the mass concentration of i-th particle fraction (three fractions are considered here); $u_{\mathrm{ri}}=u-u_{\mathrm{si}}$, $v_{\mathrm{ri}}=v-v_{\mathrm{si}}$ are the relative velocities between the two phases in the axial and radial directions, respectively. The last term in Eq.(2) models the interactions of the gas with the particle phases: $\tau_i'=\frac{\tau_i}{C_{Di}'}$ is a particle response time of the i-th particle fraction, which includes a correction for the non-Stokesian drag: $C_{Di}'=1+0.15Re_{\mathrm{si}}^{0.687}$; $\tau_i=\left(\frac{18\rho\nu}{\rho_p d_i^2}\right)^{-1}$ is a Stokesian particle response time for the i-th particle fraction with $Re_{\mathrm{si}}=\frac{d_i\sqrt{u_{\mathrm{ri}}^2+v_{\mathrm{ri}}^2}}{\nu}=\frac{d_i|\vec{V}_{\mathrm{ri}}|}{\nu}$ being the particle Reynolds number, and d_i the particle equivalent diameter; $\Omega_i=\omega_{\mathrm{si}}-0.5\left(\frac{\partial v}{\partial x}-\frac{\partial u}{\partial r}\right)$ is the a relative angular velocity for the particles; the coefficient of Magnus lift force, calculated by the closure equation given in Crowe et al. (1998): $C_{\mathrm{Mi}}=\frac{\rho C_{Li}|\vec{V}_{\mathrm{ri}}|}{\rho_p\delta_i|\Omega_i|}$ with the lift coefficient calculated as $C_{Li}=\min(0.5,0.5\chi_i)$, where the parameter $\chi_i=\frac{d_i|\omega_{\mathrm{si}}|}{\|\vec{V}_{\mathrm{ri}}\|}$; finally, ρ and ρ_p are the densities of the air and the particles respectively.

2.1.3. Linear momentum equation in the transverse direction for the gaseous phase

$$\begin{aligned}&\frac{\partial}{\partial x}\left(uv-\tilde{\nu}_t\frac{\partial v}{\partial x}\right)+\frac{\partial}{r\partial r}r\left(v^2-\tilde{\nu}_t\frac{\partial v}{\partial r}\right)\\&\quad=-\frac{\partial p}{\rho\partial r}+\frac{\partial}{\partial x}\tilde{\nu}_t\frac{\partial u}{\partial r}+\frac{\partial}{r\partial r}r\tilde{\nu}_t\frac{\partial v}{\partial r}-\frac{2\tilde{\nu}_t v}{r^2}\\&\qquad-\sum_{i=1,3}\alpha_i\left(\frac{v_{\mathrm{ri}}}{\tau_i'}-(C_{\mathrm{Mi}}\Omega_i+F_{\mathrm{si}})u_{\mathrm{ri}}\right),\end{aligned} \tag{3}$$

where the symbols are the same as in Eq. (2).

2.1.4. Turbulent kinetic equation for the gaseous phase

$$\begin{aligned}&\frac{\partial}{\partial x}\left(uk-\tilde{\nu}_t\frac{\partial k}{\partial x}\right)+\frac{\partial}{r\partial r}r\left(vk-\tilde{\nu}_t\frac{\partial k}{\partial r}\right)\\&\quad=\nu_t\left\{2\left[\left(\frac{\partial u}{\partial x}\right)^2+\left(\frac{\partial v}{\partial r}\right)^2+\left(\frac{v}{r}\right)^2\right]+\left(\frac{\partial u}{\partial r}+\frac{\partial v}{\partial x}\right)^2\right\}-\varepsilon_h\\&\qquad+\sum_{i=1,3}\frac{\alpha_i}{\tau_i}\left(u_{\mathrm{ri}}^2+v_{\mathrm{ri}}^2+0.5\left(\overline{u_{\mathrm{si}}'^2}+\overline{v_{\mathrm{si}}'^2}\right)_c-\frac{k}{\left(1+\frac{\tau_i}{T_0}\right)}\right)\end{aligned} \tag{4}$$

where $k=\frac{\overline{u'^2}+\overline{v'^2}+\overline{w'^2}}{2}$ is the turbulent energy of the fluid, $\varepsilon_h=\frac{k\sqrt{k}}{L_h}$ is the rate of dissipation calculated according to a four-way coupling model (Crowe and Gillandt, 1998) using a hybrid length scale, $L_h=\frac{2L_0\bar{\lambda}}{L_0+\bar{\lambda}}$. In the last closure equation, L_0 is the integral turbulence length scale of the gaseous phase and $\bar{\lambda}=\left(\sqrt[3]{\frac{\pi\rho_p}{6\rho\sum_{i=1,3}\alpha_i}}-1\right)\frac{\sum_{i=1,3}d_i}{3}$ is an inter-particle distance; $0.5\left(\overline{u_{\mathrm{si}}'^2}+\overline{v_{\mathrm{si}}'^2}\right)_c$ is the collision kinetic energy of the solid phases, which is calculated by the method devised by Kartushinsky and Michaelides (2004); $T_0=0.3\frac{k_0}{\varepsilon_0}$ is the turbulence integral time scale in the gaseous flow. The last term in the right-hand side of Eq. (4), which describes the turbulent kinetic energy attenuation is given by the model of Pourahmadi and Humphrey (1983). The subscript c refers to the interparticle collision model that will be described in a later section.

2.1.5. Continuity equation for solids

$$\frac{\partial}{\partial x}(\alpha_i\tilde{u}_{\mathrm{si}})+\frac{\partial}{r\partial r}r(\alpha_i\tilde{v}_{\mathrm{si}})=0, \tag{5}$$

where $\tilde{u}_{\mathrm{si}}$ and $\tilde{v}_{\mathrm{si}}$ are the axial and radial components of particle velocity, which include the effects of dispersion. The axial velocity is calculated using the drift diffusion model as follows:

$$\tilde{u}_{\mathrm{si}}=u_{\mathrm{si}}-(D_{\mathrm{ti}}+D_{\mathrm{ci}}^x)\frac{\partial\ln\alpha_i}{\partial x}, \tag{6}$$

where D_{ti} and D_{ci}^x are turbulent diffusion coefficients of particles, which are computed using the model by Shraiber et al. (1990) and with the pseudo-diffusion coefficients resulting from particle collisions computed using the model by Kartushinsky and Michaelides (2004), respectively. It must be noted that the inclusion of $\tilde{u}_{\mathrm{si}}$ in the governing equation, instead of u_{si}, is one of the main differences between the two modeling approaches.

2.1.6. Momentum equation in the axial direction for the solids phases

$$\begin{aligned}&\frac{\partial}{\partial x}\alpha_i\left(u_{\mathrm{si}}\tilde{u}_{\mathrm{si}}-\nu_{\mathrm{si}}^{xx}\frac{\partial u_{\mathrm{si}}}{\partial x}\right)+\frac{\partial}{r\partial r}r\alpha_i\left(u_{\mathrm{si}}\tilde{v}_{\mathrm{si}}-\nu_{\mathrm{si}}^{xr}\frac{\partial u_{\mathrm{si}}}{\partial r}\right)\\&\quad=\frac{\partial}{\partial x}\left(\alpha_i\nu_{\mathrm{si}}^{xx}\frac{\partial u_{\mathrm{si}}}{\partial x}\right)+\frac{\partial}{r\partial r}\left(r\alpha_i\nu_{\mathrm{si}}^{xr}\frac{\partial v_{\mathrm{si}}}{\partial x}\right)\\&\qquad+\alpha_i\left[\frac{u_{\mathrm{ri}}}{\tau_i'}+C_{\mathrm{Mi}}\Omega_i v_{\mathrm{ri}}-g\left(1-\frac{\rho}{\rho_p}\right)\right]\end{aligned} \tag{7}$$

2.1.7. Momentum equation in the radial direction for the solids phases

$$\begin{aligned}&\frac{\partial}{\partial x}\alpha_i\left(\tilde{u}_{\mathrm{si}}v_{\mathrm{si}}-\nu_{\mathrm{si}}^{xr}\frac{\partial v_{\mathrm{si}}}{\partial x}\right)+\frac{\partial}{r\partial r}r\alpha_i\left(v_{\mathrm{si}}\tilde{v}_{\mathrm{si}}-\nu_{\mathrm{si}}^{rr}\frac{\partial v_{\mathrm{si}}}{\partial r}\right)\\&\quad=\frac{\partial}{\partial x}\left(\alpha_i\nu_{\mathrm{si}}^{xr}\frac{\partial u_{\mathrm{si}}}{\partial r}\right)+\frac{\partial}{r\partial r}\left(r\alpha_i\nu_{\mathrm{si}}^{rr}\frac{\partial v_{\mathrm{si}}}{\partial x}\right)-\frac{2\alpha_i\nu_{\mathrm{si}}^{rr}v_{\mathrm{si}}}{r^2}\\&\qquad+\alpha_i\left[\frac{v_{\mathrm{ri}}}{\tau_i'}-(C_{\mathrm{Mi}}\Omega_i+F_{\mathrm{si}})u_{\mathrm{ri}}\right]\end{aligned} \tag{8}$$

where ν_{si}^{xx}, ν_{si}^{xr} and ν_{si}^{rr} are the pseudo-viscosity coefficients, which are due to interparticle collisions in the longitudinal and transverse

directions. These coefficients have been obtained analytically from the original collision model (Kartushinsky and Michaelides, 2004). F_{si} is the coefficient for the Saffman lift force, which is due to the fluid shear and is calculated from the closure equation:

$$F_{si} = \frac{3.07 \cdot \rho\psi_i}{\rho_p d_i}\sqrt{\frac{\nu}{|\mathrm{rot}\vec{V}|}}(\mathrm{rot}\vec{V})_r, \tag{9}$$

with the curl of the gas-phase velocity vector given by the expression:

$$\mathrm{rot}\vec{V} = \nabla\times\vec{V} = \left(\frac{\partial(rw)}{r\partial r} - \frac{\partial v}{r\partial\varepsilon}\right)_x \vec{i} + \left(\frac{\partial u}{r\partial\varepsilon} - \frac{\partial w}{\partial x}\right)_r \vec{j} + \left(\frac{\partial v}{\partial x} - \frac{\partial u}{\partial r}\right)_\varepsilon \vec{k} \equiv \left(\frac{\partial v}{\partial x} - \frac{\partial u}{\partial r}\right)_\varepsilon \vec{k}, \tag{10}$$

here $\vec{i}, \vec{j}$ and $\vec{k}$ are ort-vectors in the cylindrical coordinates, ε is circumferential coordinate and w is circumferential velocity component.

The correction coefficient, ψ_i was obtained by Mei (1992):

$$\psi_i = \begin{cases} 1 - 0.3314\sqrt{\beta}\exp(-0.1Re_{si}) + 0.3314\sqrt{\beta} & Re_{si} \leqslant 40 \\ 0.0524\sqrt{\beta Re_{si}} & Re_{si} > 40 \end{cases} \quad \text{with} \quad \beta = \frac{d_i|\mathrm{rot}\vec{V}|}{2|\vec{V}_{ri}|} \tag{11}$$

2.1.8. Angular momentum equation in the longitudinal direction for the solids phase

$$\frac{\partial}{\partial x}\alpha_i\left(\omega_{si}\tilde{u}_{si} - \nu_{si}^{\omega,x}\frac{\partial\omega_{si}}{\partial x}\right) + \frac{\partial}{r\partial r}r\alpha_i\left(\omega_{si}\tilde{v}_{si} - \nu_{si}^{\omega,r}\frac{\partial\omega_{si}}{\partial r}\right) = -\alpha_i C_{\omega i}\frac{\Omega_i}{\tau_i} \tag{12}$$

Both pseudo-viscosity coefficients $\nu_{si}^{\omega,x}$ and $\nu_{si}^{\omega,r}$ are calculated using formulae from Kartushinsky and Michaelides, 2004. The torque coefficient, $C_{\omega i}$ is determined as $C_{\omega i} = \frac{10}{3}$ (Rubinow and Keller, 1961; Michaelides, 2006).

2.2. Boundary conditions for the RANS model

The boundary conditions of the model are as follows:

2.2.1. In the axial direction at the pipe exit

$$\frac{\partial u}{\partial x} = \frac{\partial v}{\partial x} = \frac{\partial u_{si}}{\partial x} = \frac{\partial v_{si}}{\partial x} = \frac{\partial\omega_{si}}{\partial x} = \frac{\partial\alpha_i}{\partial x} = \frac{\partial k}{\partial x} = 0 \tag{13}$$

2.2.2. Inlet boundary (x = 0)

It is assumed that the particles enter into a well-developed, and previously computed, single-phase velocity field with an initial velocity lag determined by a coefficient K_{lag}:

$$u_{si} = K_{lag}u, \quad v_{si} = K_{lag}v, \quad \omega_{si} = K_{lag}(0.5rot\,\vec{v}). \tag{14}$$

K_{lag} is an average velocity lag (or velocity slip) that is necessary to be defined at the beginning of the computations, $L/D = 0$, and we have chosen a simple expression for it. Since the results presented have been computed at $L/D = 200$, the effects of this empirical coefficient have faded in all the results presented here.

2.2.3. Wall and centerline conditions

The no-slip condition is applied at the wall, while at the center the axisymmetric conditions are applied:

$$r = 0: \quad \frac{\partial u}{\partial r} = \frac{\partial k}{\partial r} = \frac{\partial u_{si}}{\partial r} = \frac{\partial\alpha_i}{\partial r} = v = v_{si} = \omega_{si} = 0 \tag{15}$$

$$r = R: \quad u = v = k = 0 \tag{16}$$

We prescribed the slip boundary conditions for the dispersed phase according to the model by Ding et al. (1993) as the first step in the computations (Eq. (17)). Subsequently and after the particle collisions with the walls we follow the procedure by Matsumoto and Saito (1970) to determine the particle–wall interactions. Accordingly, we have two cases of particle–wall interactions: (a) sliding collisions (Eq. (19)), and (b) non-sliding collisions (20). These two cases are characterized by the coefficients of restitution, κ_n and friction, f.

For *sliding collisions* we have the wall boundary condition:

$$r = R: \quad u_{si} = -\lambda_i\frac{\partial u_{si}}{\partial r}, \quad v_{si} = -\lambda_i\frac{\partial v_{si}}{\partial r}, \quad \omega_{si} = \lambda_i\frac{\partial\omega_{si}}{\partial r}, \tag{17}$$

where the interparticle spacing is given by the closure equation:

$$\lambda_i = d_i\left\{\left[\frac{\pi}{6}\left(\frac{\rho_p}{\rho\alpha_i} + 1\right)\right]^{1/3} - 1\right\}. \tag{18}$$

If the transverse particle velocity is positive ($v_{si} > 0$) the correction suggested by Matsumoto and Saito (1970) is used. Therefore, if $|u_{si} - 0.5d_i\omega_{si}| > 3.5\mu_0(1+\kappa_n)v_{si}$ the sliding collisions boundary conditions are as follows:

$$(a)\ u'_{si} = u_{si} + \mu_d\,\mathrm{sign}(u_{si} - 0.5d_i\omega_{si})v_{si}, \quad \omega'_{si} = \omega_{si} + \left(5\mu_d\,\mathrm{sign}(u_{si} - 0.5d_i\omega_{si})\frac{v_{si}}{d_i}\right), \quad v'_{si} = \kappa_n v_{si} \tag{19}$$

For *non-sliding collisions* the condition $|u_{si} - 0.5d_i\omega_{si}| \leqslant 3.5\mu_0(1+\kappa_n)v_{si}$ is satisfied and the boundary conditions of the dispersed phases at the wall may be written as:

$$(b)\ u'_{si} = u_{si} - \frac{2}{7}(u_{si} - 0.5d_i\omega_{si}), \quad \omega'_{si} = \omega_{si} + \frac{10(u_{si} - 0.5d_i\omega_{si})}{7d_i}, \quad v'_{si} = \kappa_n v_{si} \tag{20}$$

where the primes denote that the corresponding variables are to be calculated post-collision. The coefficients μ_d and μ_o are the kinetic (or dynamic) and static friction coefficients defined by Matsumoto and Saito (1970) and given the values $\mu_d = 0.4$ and $\mu_o = 0.8$. The coefficient f which appears in the inter-particle collision model is not related to these two coefficients.

Three groups of empirical coefficients appear in the RANS model. The first group stems from the k–ε model, which is modified according to the method by Crowe and Gillandt (1998) and takes into account the particle concentration by the use of a hybrid length scale (Michaelides, 2006). The second stems from the use of the Matsumoto and Saito (1970) model of particle–wall interactions, which introduces the dynamic and static friction coefficients. The third group accounts for the inter-particle collisions (Kartushinsky and Michaelides, 2004). All coefficients in the computations that follow were taken from the original publications and have not been modified or optimized. Also, given that this manuscript is a comparison of the results of the two modeling methods (RANS and PDF) it was not considered appropriate to optimize of make parametric studies on any of the empirical coefficients.

2.3. The probability distribution function (PDF) model

The basic premises of the PDF model for the description of dilute as well as dense dispersed multiphase systems emanate from the kinetic theory of gases: there is a strong analogy between the almost random motion of the particulate phase in turbulent multiphase flow and the random motion of molecules in a gas. For this reason, several authors applied an approach that is similar to the kinetic theory of gases in order to develop a statistical description of a dispersed particulate phase and to derive a continuum

governing equation for the flow behavior of the dispersed phase. Among these Morioka and Nakajima (1987), Reeks (1991) and Zaichik and Vinberg (1991) proposed methods for the derivation of such conservation equations from statistical principles. Simonin (2001) and Fevrier and Simonin (2001) presented reviews of the method. In this paper we use the formulation by Zaichik and Vinberg (1991) with the addition of the effect of particulate collisions.

The effect of the binary collisions of particles stems from the contribution of the collisions to the fluctuating velocities of the particles. Following the method by Zaichik et al. (2007), we consider both the isotropic collisions (which are denoted by the subscript 0 in the equations that follow) as well as the anisotropic collisions (which are denoted by the subscript 1). We consider the motion and present results obtained for both small and relatively large particles. Thus, the PDF equations for mass, momentum and the equations for the Reynolds stresses of the dispersed phase for a binary mixture ($i = 1,2$) are given in detailed description as follows in order to facilitate the use of approach which is presented in generalized form in (Zaichik et al., 2007):

2.3.1. Continuity equation

$$\frac{\partial \alpha \tilde{u}_{si}}{\partial x} + \frac{\partial (r\alpha \tilde{v}_{si})}{r\partial r} = 0 \tag{21}$$

2.3.2. Linear momentum equation in the axial direction

$$\frac{\partial}{\partial x}\alpha_i\left(u_{si}\tilde{u}_{si} + \overline{u'^2_{si}}\right) + \frac{\partial}{r\partial r} r\alpha_i\left(u_{si}\tilde{v}_{si} + \overline{u'_{si}v'_{si}}\right) = \alpha_i\left(\frac{u_{ri}}{\tau'_i} - g\right) - \left(\overline{u'^2_{si}} + G^n_{ui}\overline{u'^2}\right)\frac{\partial \alpha_i}{\partial x} - \left(\overline{u'_{si}v'_{si}} + G^n_{ui}\overline{u'v'}\right)\frac{\partial \alpha_i}{\partial r} + \alpha_i C_{xi} \tag{22}$$

where g is the gravitational acceleration as above and the coefficients G^n_{ui} denote the relaxation parameters. It must be noted that the relaxation parameters are sometimes denoted as g^n_{ui}. We have chosen the capital G in order to differentiate these parameters from the gravitational acceleration.

2.3.3. Linear momentum equation in the radial direction

$$\frac{\partial}{\partial x}\alpha_i\left(v_{si}\tilde{u}_{si} + \overline{u'_{si}v'_{si}}\right) + \frac{\partial}{r\partial r} r\alpha_i\left(v_{si}\tilde{v}_{si} + \overline{v'^2_{si}}\right) = \frac{\alpha_i v_{ri}}{\tau'_i} - \left(\overline{u'_{si}v'_{si}} + G^l_{ui}\overline{u'v'}\right)\frac{\partial \alpha_i}{\partial x} - \left(\overline{v'^2_{si}} + G^n_{ui}\overline{v'^2}\right)\frac{\partial \alpha_i}{\partial r} + \alpha_i C_{ri} \tag{23}$$

2.3.4. Velocity fluctuations evolution equation in the axial direction

$$\begin{aligned}
&\frac{\partial}{\partial x}\alpha_i\left\{\overline{u'^2_{si}}\tilde{u}_{si} - \tau_{2i*}\left[\left(\overline{u'^2_{si}} + G^l_{ui}\overline{u'^2}\right)\frac{\partial \overline{u'^2_{si}}}{\partial x} + \left(\overline{u'_{si}v'_{si}} + G^n_{ui}\overline{u'v'}\right)\frac{\partial \overline{u'^2_{si}}}{\partial r}\right]\right\} \\
&+ \frac{\partial}{r\partial r} r\alpha_i\left\{\overline{u'^2_{si}}\tilde{v}_{si} - \frac{\tau_{2i*}}{3}\left[\left(\overline{u'_{si}v'_{si}} + G^l_{ui}\overline{u'v'}\right)\frac{\partial \overline{u'^2_{si}}}{\partial x} + \left(\overline{v'^2_{si}} + G^n_{ui}\overline{v'^2}\right)\frac{\partial \overline{u'^2_{si}}}{\partial r} + 2\left(\left(\overline{u'^2_{si}} + G^l_{ui}\overline{u'^2}\right)\frac{\partial \overline{u'_{si}v'_{si}}}{\partial x} + \left(\overline{u'_{si}v'_{si}} + G^n_{ui}\overline{u'v'}\right)\frac{\partial \overline{u'_{si}v'_{si}}}{\partial r}\right)\right]\right\} \\
&= -2\left\{\left(\overline{u'^2_{si}} + G^l_{ui}\overline{u'^2}\right)\frac{\partial u_{si}}{\partial r} - l^l_{ui}\overline{u'^2}\frac{\partial u}{\partial x} - l^n_{ui}\overline{u'v'}\frac{\partial u}{\partial r} - \frac{\left(f^l_{ui}\overline{u'^2} - \overline{u'^2_{si}}\right)}{\tau'_i} + \left[\frac{\left(1-\kappa_n^2\right)}{9\tau_{ci}}\kappa_{si} + \frac{\left(\overline{u'^2_{si}} - \frac{2}{3}\kappa_{si}\right)}{\tau_{c1i}}\right]\left(1 - f^m_{ui}\right)\right\}\alpha_i \\
&+ C_{xrii} + C_{xrij}
\end{aligned} \tag{24}$$

2.3.5. Velocity fluctuations evolution equation in the radial direction

$$\begin{aligned}
&\frac{\partial}{\partial x}\alpha_i\left\{\overline{v'^2_{si}}\tilde{u}_{si} - \frac{\tau_{2i*}}{3}\left[\left(\overline{u'^2_{si}} + G^l_{ui}\overline{u'^2}\right)\frac{\partial \overline{v'^2_{si}}}{\partial x} + \left(\overline{u'_{si}v'_{si}} + G^n_{ui}\overline{u'v'}\right)\frac{\partial \overline{v'^2_{si}}}{\partial r} + 2\left(\overline{u'_{si}v'_{si}} + G^l_{ui}\overline{u'v'}\right)\frac{\partial \overline{u'_{si}v'_{si}}}{\partial x} + \left(\overline{v'^2_{si}} + G^n_{ui}\overline{v'^2}\right)\frac{\partial \overline{u'_{si}v'_{si}}}{\partial r}\right]\right\} \\
&+ \frac{\partial}{r\partial r} r\alpha_i\left\{\overline{v'^2_{si}}\tilde{v}_{si} - \tau_{2i*}\left[\left(\overline{u'_{si}v'_{si}} + G^l_{ui}\overline{u'v'}\right)\frac{\partial \overline{v'^2_{si}}}{\partial x} + \left(\overline{v'^2_{si}} + G^n_{ui}\overline{v'^2}\right)\frac{\partial \overline{v'^2_{si}}}{\partial r}\right]\right\} = \\
&-2\left\{\left(\overline{u'_{si}v'_{si}} + G^l_{ui}\overline{u'v'}\right)\frac{\partial v_{si}}{\partial x} + \left(\overline{v'^2_{si}} + G^n_{ui}\overline{v'^2}\right)\frac{\partial v_{si}}{\partial r} - l^l_{ui}\overline{u'v'}\frac{\partial v}{\partial x} - l^n_{ui}\overline{v'^2}\frac{\partial v}{\partial r} - \frac{\left(f^l_{ui}\overline{v'^2} - \overline{v'^2_{si}}\right)}{\tau'_i} + \left[\frac{\left(1-\kappa_n^2\right)}{9\tau_{ci}}\kappa_{si} + \frac{\left(\overline{v'^2_{si}} - \frac{2}{3}\kappa_{si}\right)}{\tau_{c1i}}\right]\left(1 - f^m_{ui}\right)\right\}\alpha_i \\
&+ C_{rrii} + C_{rrij}
\end{aligned} \tag{25}$$

2.3.6. Velocity fluctuations evolution equation in the circumferential direction

$$\begin{aligned}
&\frac{\partial}{\partial x}\alpha_i\left\{\overline{w'^2_{si}}\tilde{u}_{si} - \frac{\tau_{2i*}}{3}\left[\left(\overline{u'^2_{si}} + G^l_{ui}\overline{u'^2}\right)\frac{\partial \overline{w'^2_{si}}}{\partial x} + \left(\overline{u'_{si}v'_{si}} + G^n_{ui}\overline{u'v'}\right)\frac{\partial \overline{w'^2_{si}}}{\partial r}\right]\right\} \\
&+ \frac{\partial}{r\partial r} r\alpha_i\left\{\overline{w'^2_{si}}v_{si} - \frac{\tau_{2i*}}{3}\left[\left(\overline{u'_{si}v'_{si}} + G^l_{ui}\overline{u'v'}\right)\frac{\partial \overline{w'^2_{si}}}{\partial x} + \left(\overline{v'^2_{si}} + G^n_{ui}\overline{v'^2}\right)\frac{\partial \overline{w'^2_{si}}}{\partial r}\right]\right\} \\
&= 2\left\{\frac{\left(f^l_{ui}\overline{w'^2} - \overline{w'^2_{si}}\right)}{\tau'_i} - \left[\frac{\left(1-\kappa_n^2\right)}{9\tau_{ci}}\kappa_{si} + \frac{\left(\overline{w'^2_{si}} - \frac{2}{3}\kappa_{si}\right)}{\tau_{c1i}}\right]\left(1 - f^m_{ui}\right)\right\}\alpha_i \\
&+ C_{zzii} + C_{zzij}
\end{aligned} \tag{26}$$

2.3.7. Reynolds stress fluctuations evolution equation

$$\begin{aligned}
&\frac{\partial}{\partial x}\alpha_i\left\{\overline{u'_{si}v'_{si}}\tilde{u}_{si} - \frac{\tau_{2i*}}{3}\left[2\left(\left(\overline{u'^2_{si}} + G^l_{ui}\overline{u'^2}\right)\frac{\partial \overline{u'_{si}v'_{si}}}{\partial x} + \left(\overline{u'_{si}v'_{si}} + G^n_{ui}\overline{u'v'}\right)\frac{\partial \overline{u'_{si}v'_{si}}}{\partial r}\right) + \left(\overline{u'_{si}v'_{si}} + G^l_{ui}\overline{u'v'}\right)\frac{\partial \overline{u'^2_{si}}}{\partial x} + \left(\overline{u'_{si}v'_{si}} + G^n_{ui}\overline{u'v'}\right)\frac{\partial \overline{v'^2_{si}}}{\partial r}\right]\right\} \\
&+ \frac{\partial}{r\partial r} r\alpha_i\left\{\overline{u'_{si}v'_{si}}\tilde{v}_{si} - \tau_{2i*}\left[2\left(\left(\overline{u'_{si}v'_{si}} + G^l_{ui}\overline{u'v'}\right)\frac{\partial \overline{u'_{si}v'_{si}}}{\partial x} + \left(\overline{v'^2_{si}} + G^n_{ui}\overline{v'^2}b\right)\times\frac{\partial \overline{u'_{si}v'_{si}}}{\partial r}\right) + \left(\overline{u'^2_{si}} + G^l_{ui}\overline{u'^2}\right)\frac{\partial \overline{v'^2_{si}}}{\partial x} + \left(\overline{u'_{si}v'_{si}} + G^n_{ui}\overline{u'v'}\right)\frac{\partial \overline{v'^2_{si}}}{\partial r}\right]\right\} = \\
&-\left\{\left(\overline{u'_{si}v'_{si}} + G^l_{ui}\overline{u'v'}\right)\frac{\partial u_{si}}{\partial x} + \left(\overline{v'^2_{si}} + G^n_{ui}\overline{v'^2}\right)\times\frac{\partial u_{si}}{\partial r} + \left(\overline{u'^2_{si}} + G^l_{ui}\overline{u'^2}\right)\frac{\partial v_{si}}{\partial x} + \left(\overline{u'_{si}v'_{si}} + G^n_{ui}\overline{u'v'}\right)\frac{\partial v_{si}}{\partial r} - l^l_{ui}\overline{u'^2}\frac{\partial v}{\partial x} - l^n_{ui}\overline{u'v'}\frac{\partial v}{\partial r}\right. \\
&\left. - l^l_{ui}\overline{u'v'}\frac{\partial u}{\partial x} - l^l_{ui}\overline{v'^2}\frac{\partial u}{\partial r} - \frac{\left(f^l_{ui} + f^n_{ui}\right)\overline{u'v'} - 2\overline{u'_{si}v'_{si}}}{\tau'_i} + \frac{2\left(1 - f^m_{ui}\right)}{\tau_{c1i}}\overline{u'_{si}v'_{si}}\right\}\alpha_i \\
&+ C_{xrii} + C_{xrij}
\end{aligned} \tag{27}$$

where the binary collision terms on the right-hand side of Eqs. (22)–(27) may be decomposed into two terms and are calculated by the following expressions:

$$C_{xi} = C^0_{xi} + C^1_{xi}, \quad C_{ri} = C^0_{ri} + C^1_{ri}, \quad C_{xxi} = C^0_{xxi} + C^1_{xxi}, \quad C_{rri} = C^0_{rri} + C^1_{rri}, \quad C_{xri} = C^0_{xri} + C^1_{xri} \tag{28}$$

$$C^0_{xi} = \frac{\pi\sigma^2\rho\alpha_j(1+\kappa_n)W}{2(m_i+m_j)}W_{sx}F_1(z) \tag{29}$$

$$C^0_{xj} = \frac{\pi\sigma^2\rho\alpha_i(1+k_n)W}{2(m_i+m_j)}W_{sr}F_1(z) \tag{30}$$

$$C^1_{xi} = \frac{\pi\sigma^2\rho\alpha_j(1+k_n)w'^4}{2(m_i+m_j)W^2} \times\left[W(B_{xx}W_x + B_{xr}W_r)\Psi_1 - \frac{W_xW_r(B_{rx}W_x+B_{rr}W_r)}{2W}\Psi_2(z)\right], \quad (31)$$

$$C^1_{ri} = \frac{\pi\sigma^2\rho\alpha_j(1+k_n)w'^4}{2(m_i+m_j)W^2} \times\left[W(B_{rx}W_x + B_{rr}W_r)\Psi_1 - \frac{W_xW_y(B_{xx}W_x+B_{xr}W_r)}{2W}\Psi_2(z)\right], \quad (32)$$

$$C^0_{xxi} = \frac{\pi\sigma^2\rho\alpha_j(1+k_n)W}{(m_i+m_j)} \times\left\{\frac{m_j(1+k_n)}{4(m_i+m_j)}\left[\left(W^2_{sx}+\frac{W^2}{3}\right)F_2(z) - \left(W^2_{sx}-\frac{W^2}{3}\right)\frac{3F_1(z)}{2z}\right] -\kappa_i\left[W^2_{sx}\frac{2F_0(z)}{z} - \left(W^2_{sx}-\frac{W^2}{3}\right)\frac{3F_1(z)}{2z}\right]\right\}, \quad (33)$$

$$C^0_{rri} = \frac{\pi\sigma^2\rho\alpha_j(1+\kappa_n)W}{(m_i+m_j)} \times\left\{\frac{m_j(1+\kappa_n)}{4(m_i+m_j)}\left[\left(W^2_{sr}+\frac{W^2}{3}\right)F_2(z) - \left(W^2_{sr}-\frac{W^2}{3}\right)\frac{3F_1(z)}{2z}\right] -\kappa_i\left[W^2_{sr}\frac{2F_0(z)}{z} - \left(W^2_{sr}-\frac{W^2}{3}\right)\frac{3F_1(z)}{2z}\right]\right\}, \quad (34)$$

$$C^0_{xri} = \frac{\pi\sigma^2\rho\alpha_j(1+\kappa_n)W}{(m_i+m_j)} \left\{\frac{m_j(1+\kappa_n)}{4(m_i+m_j)}\left[\left(W_{sx}W_{sr}+\frac{W^2}{3}\right)F_2(z) - \left(W_{sx}W_{sr}-\frac{W^2}{3}\right)\frac{3F_1(z)}{2z}\right] -\kappa_i\left[W_{sx}W_{sr}\frac{2F_0(z)}{z} - \left(W_{sx}W_{sr}-\frac{W^2}{3}\right)\frac{3F_1(z)}{2z}\right]\right\}, \quad (35)$$

$$C^1_{xxi} = \frac{\pi\sigma^2\rho\alpha_j(1+\kappa_n)^2m_j^2W}{4(m_i+m_j)^2}\left\{2w'^4B_{xx}\Psi_3(z) + w'^2\left[W^2_{sx}B_{xx} + 2W_{sx}W_{sr}B_{xr} + W^2_{sr}B_{rr} + 4(W_{sx}(B_{rx}W_{sx}+B_{rr}W_{sr}))\right]\frac{\Psi_4(z)}{2z} - W^2_{sx}(W^2_{sx}B_{xx} + 2W_{sx}W_{sr}B_{xr} + W^2_{sr}B_{rr})\frac{\Psi_5(z)}{4z^2}\right\} - \frac{\pi\sigma^2\rho\alpha_j(1+k_n)m_jW}{(m_i+m_j)}\left\{\kappa_i\left[2w'^4B_{xx}\times\Psi_3(z) - w'^2(W^2_{sx}B_{xx} + 2W_{sx}W_{sr}B_{xr} + W^2_{sr}B_{rr})\frac{\Psi_2(z)}{4z^2} + 2w'^2(W_{sx}(B_{rx}W_{sx}+B_{rr}W_{sr}))\frac{\Psi_6(z)}{2z} - W^2_{sx}\times(W^2_{sx}B_{xx} + 2W_{sx}W_{sr}B_{xr} + W^2_{sr}B_{rr})\frac{\Psi_7(z)}{2z^2}\right] - \frac{\overline{k^2_{si}k^2_{sj}}}{w'^4}2(1-\zeta^2_{12}) \times\left[w'^4E_{xx}F_1(z) + w'^2W_{sx}(E_{xr}W_{sx}+E_{rr}W_{sr})\frac{\Psi_1(z)}{2z}\right]\right\}, \quad (36)$$

$$C^1_{rri} = \frac{\pi\sigma^2\rho\alpha_j(1+\kappa_n)^2m_j^2W}{4(m_i+m_j)^2}\left\{2w'^4B_{rr}\Psi_3(z) + w'^2\left[W^2_{sx}B_{xx} + 2W_{sx}W_{sr}B_{xr} + W^2_{sr}B_{rr} + 4(W_{sr}(B_{rx}W_{sx}+B_{rr}W_{sr}))\right]\frac{\Psi_4(z)}{2z} - W^2_{sr}(W^2_{sx}B_{xx} + 2W_{sx}W_{sr}B_{xr} + W^2_{sr}B_{rr})\frac{\Psi_5(z)}{4z^2}\right\} - \frac{\pi\sigma^2\rho\alpha_j(1+\kappa_n)m_jW}{(m_i+m_j)}\left\{\kappa_i\left[2w'^4B_{rr}\times\Psi_3(z) - w'^2(W^2_{sx}B_{xx} + 2W_{sx}W_{sr}B_{xr} + W^2_{sr}B_{rr})\frac{\Psi_2(z)}{4z^2} + 2w'^2(W_{sr}(B_{rx}W_{sx}+B_{rr}W_{sr}))\frac{\Psi_6(z)}{2z} - W^2_{sr}\times(W^2_{sx}B_{xx} + 2W_{sx}W_{sr}B_{xr} + W^2_{sr}B_{rr})\frac{\Psi_7(z)}{2z^2}\right] - \frac{\overline{k^2_{si}k^2_{sj}}}{w'^4} \times 2(1-\zeta^2_{12})\left[w'^4E_{rr}F_1(z) + w'^2W_{sr}(E_{xr}W_{sx}+E_{rr}W_{sr})\times\frac{\Psi_1(z)}{2z}\right]\right\}, \quad (37)$$

$$C^1_{xri} = \frac{\pi\sigma^2\rho\alpha_j(1+\kappa_n)^2m_j^2W}{4(m_i+m_j)^2}\left\{2w'^4B_{xx}\Psi_3(z) + w'^2[(W_{sx}(B_{rx}W_{sx}+B_{rr}W_{sr}) + W_{sr}(B_{xx}W_{sx}+B_{xr}W_{sr}))]\times\frac{\Psi_4(z)}{z} - W_{sx}W_{sr}(W^2_{sx}B_{xx} + 2W_{sx}W_{sr}B_{xr} + W^2_{sr}B_{rr})\frac{\Psi_5(z)}{4z^2}\right\} - \frac{\pi\sigma^2\rho\alpha_j(1+\kappa_n)m_jW}{(m_i+m_j)} \times\left\{\kappa_i\left[2w'^4B_{xr}\Psi_3(z) + w'^2(W_{sx}(B_{rx}W_{sx}+B_{rr}W_{sr}) + W_{sr}(B_{xx}W_{sx} + B_{xr}W_{sr}))\frac{\Psi_6(z)}{4z^2} - W_{sx}(W^2_{sx}B_{xx} + 2W_{sx}W_{sr}B_{xr} + W^2_{sr}B_{rr})\times W_{sr}\frac{\Psi_7(z)}{2z^2}\right] - \frac{\overline{k^2_{si}k^2_{sj}}}{w'^4}(1-\zeta^2_{12})[2w'^4E_{xr}F_1(z) + w'^2(W_{sx}(E_{xr}W_{sx}+E_{rr}W_{sr}) + W_{sr}(E_{xx}W_{sx}+E_{xr}W_{sr}))\times\frac{\Psi_1(z)}{2z}]\right\}, \quad (38)$$

The definition and closure equations of the additional parameters used in the expressions (22)–(38) are as follows:

$$k_{si} = \frac{\overline{u'^2_{si}} + \overline{v_{si}}'^2}{2}, \quad f_{uxi} = \frac{T^x_{Lpi}}{\tau'_i + T^x_{Lpi}}, \quad f_{uri} = \frac{T^r_{Lpi}}{\tau'_i + T^r_{Lpi}},$$

$$f_{ui} = \frac{(f_{uxi} + 2f_{uri})}{3}, \quad \zeta_{ij} = \sqrt{f_{ui}f_{uj}},$$

$$w'^2 = k_{si} + k_{sj} - 2\zeta_{ij}\sqrt{k_{si}k_{sj}}, \quad \kappa_i = \frac{k_{si} - \zeta_{ij}\sqrt{k_{si}k_{sj}}}{k_{si} + k_{sj} - 2\zeta_{ij}\sqrt{k_{si}k_{sj}}},$$

$$\kappa_j = \frac{k_{sj} - \zeta_{ij}\sqrt{k_{si}k_{sj}}}{k_{si} + k_{sj} - 2\zeta_{ij}\sqrt{k_{si}k_{sj}}},$$

$$B_{xx} = \frac{1}{2(1-\zeta^2_{ij})}\left[\frac{\kappa_i^2R_{ixx}}{k^4_{si}}\left(1+\zeta_{ij}\frac{\kappa_j\sqrt{k_{si}}}{k_i\sqrt{k_{sj}}}\right) + \frac{\kappa_j^2R_{jxx}}{k^4_{sj}}\left(1+\zeta_{ij}\frac{\kappa_i\sqrt{k_{sj}}}{k_j\sqrt{k_{si}}}\right)\right],$$

$$B_{rr} = \frac{1}{2(1-\zeta^2_{ij})}\left[\frac{\kappa_i^2R_{irr}}{k^4_{si}}\left(1+\zeta_{ij}\frac{\kappa_j\sqrt{k_{si}}}{k_i\sqrt{k_{sj}}}\right) + \frac{\kappa_j^2R_{jrr}}{k^4_{sj}}\left(1+\zeta_{ij}\frac{\kappa_i\sqrt{k_{sj}}}{k_j\sqrt{k_{si}}}\right)\right],$$

$$B_{xr} = \frac{1}{2(1-\zeta^2_{ij})}\left[\frac{\kappa_i^2R_{ixr}}{k^4_{si}}\left(1+\zeta_{ij}\frac{\kappa_j\sqrt{k_{si}}}{k_i\sqrt{k_{sj}}}\right) + \frac{\kappa_j^2R_{jxr}}{k^4_{sj}}\left(1+\zeta_{ij}\frac{\kappa_i\sqrt{k_{sj}}}{k_j\sqrt{k_{si}}}\right)\right],$$

$$E_{xx} = \frac{1}{2(1-\zeta^2_{ij})}\left[\frac{R_{jxx}}{k^4_{si}}\left(\kappa_j + \frac{\zeta_{ij}(\kappa_i-\kappa_j)\sqrt{k_{sj}}}{2\sqrt{k_{si}}}\right) - \frac{R_{ixx}}{k^4_{sj}}\left(\kappa_i + \frac{\zeta_{ij}(\kappa_j-\kappa_i)\sqrt{k_{si}}}{2\sqrt{k_{sj}}}\right)\right],$$

$$E_{rr} = \frac{1}{2(1-\zeta^2_{ij})}\left[\frac{R_{jrr}}{k^4_{si}}\left(\kappa_j + \frac{\zeta_{ij}(\kappa_i-\kappa_j)\sqrt{k_{sj}}}{2\sqrt{k_{si}}}\right) - \frac{R_{irr}}{k^4_{sj}}\left(\kappa_i + \frac{\zeta_{ij}(\kappa_j-\kappa_i)\sqrt{k_{si}}}{2\sqrt{k_{sj}}}\right)\right],$$

$$E_{xr} = \frac{1}{2(1-\zeta^2_{ij})}\left[\frac{R_{jxr}}{k^4_{si}}\left(\kappa_j + \frac{\zeta_{ij}(\kappa_i-\kappa_j)\sqrt{k_{sj}}}{2\sqrt{k_{si}}}\right) - \frac{R_{ixr}}{k^4_{sj}}\left(\kappa_i + \frac{\zeta_{ij}(\kappa_j-\kappa_i)\sqrt{k_{si}}}{2\sqrt{k_{sj}}}\right)\right].$$

Where $R_{ixx} = 0, R_{irr} = 0, R_{ixr} = \overline{u'_{si}v'_{si}}, m_i = \frac{\pi}{6}\rho_p d_i^3$ is the mass of the i-th particle and $\sigma = \frac{d_i+d_j}{2}$ is the radius of the collision sphere. The following parameters and functions are used in the application of the pdf model: $z = \frac{W^2}{2w'^2}, W_{sx} = u_{s2} - u_{s1}, W_{sr} = v_{s2} - v_{s1}, W = \sqrt{W^2_{sx} + W^2_{sr}}$.

The functions $F_i(z)$ and $\Psi_i(z)$ are as follows:

$$F_0(z)=\frac{\exp(-z)}{\sqrt{\pi z}}+\left(1+\frac{1}{2z}\right)\mathrm{erf}\sqrt{z},\psi_0(z)$$
$$=\frac{3\exp(-z)}{\sqrt{\pi z}}+\left(1-\frac{3}{2z}\right)\mathrm{erf}\sqrt{z},$$
$$F_1(z)=\left(1+\frac{1}{2z}\right)\frac{\exp(-z)}{\sqrt{\pi z}}+\left(1+\frac{1}{z}-\frac{1}{4z^2}\right)\mathrm{erf}\sqrt{z},\Psi_1(z)$$
$$=4F_0(z)-3F_1(z),\Psi_2(z)=\Psi_1(z)-\frac{2\Psi_0(z)}{z},$$
$$F_2(z)=F_1(z)+\frac{2F_0(z)}{z},\Psi_3(z)=F_1(z)+\frac{2\Psi_1(z)}{z},$$
$$\Psi_4(z)=\Psi_1(z)-\frac{\Psi_2(z)}{2z},\Psi_5(z)=\Psi_1(z)-\frac{7\Psi_2(z)}{2z},$$
$$\Psi_6(z)=\Psi_1(z)-\frac{\Psi_2(z)}{z},\Psi_7(z)=\frac{\Psi_2(z)+\Psi_5(z)}{2}$$

where $\overline{u'_{\mathrm{si}}v'_{\mathrm{si}}}$ is the cross-correlation velocity of the i-th fraction of the dispersed phase; $\overline{u'^2_{\mathrm{si}}}$, $\overline{v'^2_{\mathrm{si}}}$ and $\overline{w'^2_{\mathrm{si}}}$ are the velocity correlations in axial, radial and circumferential directions, respectively. All these velocity correlations are computed taking into account the collisions of the particles and the evolution of the collision velocities into turbulent motion.

2.4. Boundary conditions for the PDF model

The boundary conditions at the axis of the pipe ($r = 0$) are:

$$\frac{\partial u_{\mathrm{si}}}{\partial r}=v_{\mathrm{si}}=\frac{\partial\overline{u'^2_{\mathrm{si}}}}{\partial r}=\frac{\partial\overline{v'^2_{\mathrm{si}}}}{\partial r}=\frac{\partial\overline{w'^2_{\mathrm{si}}}}{\partial r}=\overline{u'_{\mathrm{si}}v'_{\mathrm{si}}}=0 \tag{39}$$

The boundary conditions at the wall ($r = R$) are:

$$\tau'_i\frac{\partial u_{\mathrm{si}}}{\partial r}=2\frac{(1-\kappa_x)}{(1+\kappa_x)}u_s\sqrt{\frac{2}{\pi\overline{v'^2_{\mathrm{si}}}}} \tag{40}$$
$$v_{\mathrm{si}}=0 \tag{41}$$
$$\tau'_i\frac{\partial\overline{u'^2_{\mathrm{si}}}}{\partial r}=3\frac{(1-\kappa_x^2)}{(1+\kappa_x^2)}\overline{u'^2_{\mathrm{si}}}\sqrt{\frac{2}{\pi\overline{v'^2_{\mathrm{si}}}}} \tag{42}$$
$$\tau'_i\frac{\partial\overline{v'^2_{\mathrm{si}}}}{\partial r}=2\frac{(1-\kappa_n^2)}{(1+\kappa_n^2)}\sqrt{\frac{2\overline{v'^2_{\mathrm{si}}}}{\pi}} \tag{43}$$
$$\tau'_i\frac{\partial\overline{w'^2_{\mathrm{si}}}}{\partial r}=0 \tag{44}$$
$$\overline{u'_{\mathrm{si}}v'_{\mathrm{si}}}=-\mu_x\overline{v'^2} \tag{45}$$

2.5. Other closure equations that have been used in the PDF model

Several time scales are used with the PDF models. Their closure equations may be summarized as follows:

The inter-particle collision times, τ_{ci}, τ_{c1i}, and τ_{c2i} are as follows: $\tau_{\mathrm{ci}}=\left(\frac{2\pi}{3k_{\mathrm{si}}}\right)^{1/2}\frac{d_i}{16\alpha(1-f_{\mathrm{ui}}^m)^{0.5}}$, $\tau_{c1i}=\left(\frac{2\pi}{3k_{\mathrm{si}}}\right)^{1/2}\frac{5d_i}{8\alpha(1+k_n)(3-k_n)(1-f_{\mathrm{ui}}^m)^{0.5}}$, and $\tau_{c2i}=\left(\frac{2\pi}{3k_{\mathrm{si}}}\right)^{1/2}\frac{45d_i}{4\alpha_i(1+k_n)(49-33k_n)(1-f_{\mathrm{ui}}^m)^{0.5}}$. The average time that elapses between collisions τ'_i and τ_{c2i} is: $\tau_{2i*}:\tau_{2i*}=\frac{\tau'_i\tau_{c2i}}{\tau_{c2i}+(1-f_{\mathrm{ui}}^m)\tau'_i}$.

The particle response time: $\tau'_i=\frac{\rho_p d_i^2}{18\mu C'_{Di}}$, and with the corrections for non-Stokesian drag $C'_{Di}=1+0.15Re_{\mathrm{si}}^{0.687}$, for $Re_s\leqslant 10^3$and $C'_{Di}=0.11\frac{Re_{\mathrm{si}}}{6}$ for $Re_{\mathrm{si}}>10^3$.

The time of particle interactions with the turbulent eddies has been calculated according to the method proposed by Wang and Stock (1993):

$$T^l_{\mathrm{Lpi}}=\frac{T_{\mathrm{Lpi}}}{\sqrt{1+(m_{\mathrm{Ti}}\gamma_i)^2}},T^n_{\mathrm{Lpi}}=\frac{2\sqrt{1+(m_{\mathrm{Ti}}\gamma_i)^2}-m_{\mathrm{Ti}}\gamma_i}{\sqrt{1+(m_{\mathrm{Ti}}\gamma_i)^2}}T_{\mathrm{Lpi}},T^m_{\mathrm{Lpi}}=\frac{T^l_{\mathrm{Lpi}}+2T^n_{\mathrm{Lpi}}}{3}$$

The model coefficients that accounts for the effect of turbulence on the motion of the particles are: $f^\varsigma_{\mathrm{ui}}=\frac{2\Omega_{\varsigma i}+Z^2_{\varsigma i}}{2\Omega_{\varsigma i}+2\Omega^2_{\varsigma i}+Z^2_{\varsigma i}}$, $g^\varsigma_{\mathrm{ui}}=\frac{1}{\Omega_{\varsigma i}}-f^\varsigma_{\mathrm{ui}}$, $l^\varsigma_{\mathrm{ui}}=g^\varsigma_{\mathrm{ui}}-\frac{(2\Omega_{\varsigma i}+Z^2_{\varsigma i})^2-2\Omega^2_{\varsigma i}Z^2_{\varsigma i}}{(2\Omega_{\varsigma i}+2\Omega^2_{\varsigma i}+Z^2_{\varsigma i})^2}$, with $\Omega_{\varsigma i}=\frac{\tau'_i}{T^\varsigma_{\mathrm{Lpi}}}$, $Z_{\varsigma i}=\frac{\tau_T}{T^\varsigma_{\mathrm{Lpi}}}$, $\varsigma=l,n,m$, are orientation along x, r and z directions, correspondingly. Other parameters that have been used in the computations of this paper are as follows:

$$m_{Ti}=\frac{T_{\mathrm{Lpi}}}{T_E}=F(St_{\mathrm{Ei}}),\quad T_{\mathrm{Lpi}}=F(St_{\mathrm{Ei}})T_E,\quad T_E=2.81T_L,$$
$$F(St_{\mathrm{Ei}})=1-\frac{0.644}{(1+St_{\mathrm{Ei}})^{0.4(1+0.01St_{\mathrm{Ei}})}},\quad St_{\mathrm{Ei}}=\frac{\tau'_i}{T_E},$$
$$\gamma=\frac{|u-u_s|}{\sqrt{2k/3}}\equiv\frac{|u_r|}{\sqrt{2k/3}}.$$

The Lagrange integral time scale is defined as: $T_L=\sqrt{\left(\frac{10\nu}{u_*^2}\right)^2+\left(\varsigma\frac{k}{\varepsilon}\right)^2}$, with $\varsigma=C_\mu^{0.5}=0.3$. The Taylor time scale is: $\tau_T=\sqrt{\frac{2Re_\lambda}{a_0\sqrt{15}}}\tau_K$, with $Re_\lambda=\sqrt{\frac{20k^2}{3\varepsilon\nu}}$, $\tau_K=\sqrt{\frac{\nu}{\varepsilon}}$, and $a_0=\frac{11+7Re_\lambda}{205+Re_\lambda}$.

The restitution coefficient of particles in the longitudinal direction during the collisions is:

$$k_x=\begin{cases}1-\xi_x,0\leqslant\xi_x\leqslant\frac{2}{7}\\ \frac{5}{7},\xi_x>\frac{2}{7}\end{cases},\quad\text{where}\quad\xi_x=\mu_x(1+\kappa_x)\tan\left|\frac{v_{\mathrm{si}}}{u_{\mathrm{si}}}\right|,$$

The turbulent kinetic energy of the particles is: $k_{\mathrm{si}}=0.5(\overline{u'^2_{\mathrm{si}}}+\overline{v'^2_{\mathrm{si}}}+\overline{w'^2_{\mathrm{si}}})$.

We have used the standard notation in the closure equations for the PDF model. Thus, among the symbols that have been used: St_E is the Stokes number; T_E is the Euler integral time scale; u_* is the friction velocity; γ is the so-called "drift parameter;" is the rate of turbulent kinetic energy dissipation; μ_x is the friction coefficient for the particle interactions with the wall; and $\tau_K$is the Kolmogorov microtime scale. As with the RANS method all coefficients that appear in the PDF model are the same as in the original publication by Zaichik et al. (2007).

3. Numerical method

In the RANS and PDF computations the *control volume* method was used. The governing equations were solved using the ILU method, which incorporates a strong implicit procedure with lower and upper matrix decomposition and with an up-wind scheme. For the computations presented in this paper, 600,000 uniformly sized volumes were used. The wall functions, obtained from Peric and Scheuerer (1989) were incorporated at a dimensionless distance $y_+ = 11$ from the wall. All computations were extended from the pipe entrance to a distance $x/D = 200$, where the results reach quasi-steady conditions and the entrance effects have faded. For the particulate phases, where the size of particles is often larger than the size of the viscous boundary sublayer, we employed the numerical method developed by Hussainov et al. (1996) and used wall functions that took into account the size of the particles.

We conducted an extensive grid uncertainty study and concluded that the 600,000 ($40\times 15{,}000$) volumes grid is adequate for the control volume computations of this study. This type of grid spacing in the transverse direction is approximately 50% larger than the diameters of the larger particles used. Using a denser grid of 937,500 points ($50\times 18{,}750$) showed less than 0.5% deviation in the gas and solids velocity profile results, less than and less than 0.6% deviation in the solids velocity profile results and less than

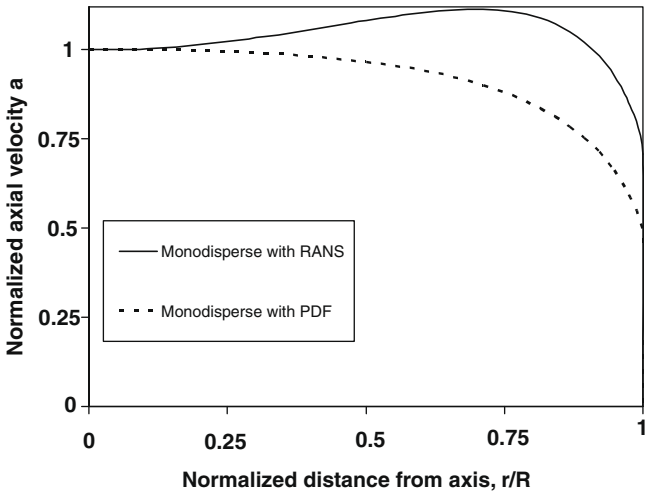

Fig. 1. Axial velocity profile of the carrier phase with monodisperse particles of 0.5 mm.

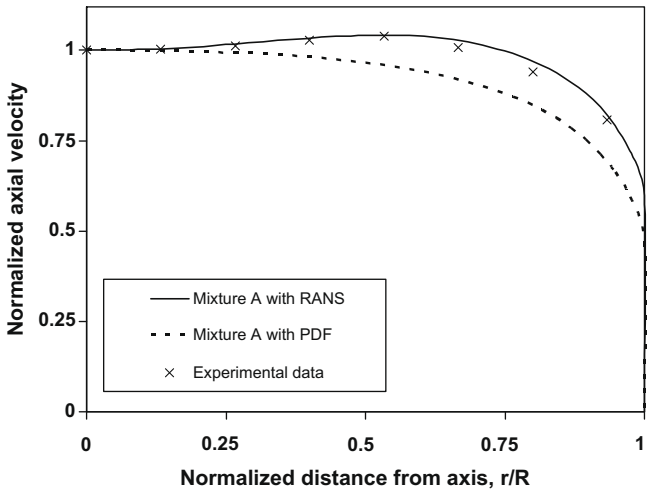

Fig. 2. Axial velocity profile of air with a solids mixture composed of equal parts of spheres with diameters 0.50, 0.45 and 0.55 mm. The experimental data are from Tsuji et al. (1984).

0.5% deviation in the solids fraction concentration results. However, a significantly lighter grid with 322,000 ($28 \times 11{,}500$) volumes showed a much lower fidelity, with maximum deviations of 4.5% for solids and gas velocities and 5.2% for solids fraction concentration profiles. In general, all grid sensitivity computations that were conducted proved that the $40 \times 15{,}000$ grid is adequate for the computation of accurate results from this model.

4. Results and discussion

All the numerical results that are presented in the following paragraphs were obtained at a distance of 200 diameters from the entrance of the channel, where quasi-steady flow conditions have been achieved. Whenever possible, the results are presented in dimensionless form. The centerline axial gas velocity u_m has been used to make the gas and the solids velocities dimensionless. The square of this velocity was used to normalize the turbulent kinetic energies. The properties of the particles used in the computations are those of polystyrene with material density $\rho_p = 1000\ \mathrm{kg/m^3}$. The pipe diameter is $D = 30.5$ mm and, at an average gas average velocity $\bar{u} = 11$ m/s the Reynolds number of the flow is: $Re = 2.2 \cdot 10^4$. The solids loading is 3.4 in all cases unless indicated otherwise.

Fig. 1 shows the normalized axial velocity of the gas-phase obtained by using the two methods. It is observed that the results of the PDF method show the typical channel flow profile, while those obtained by the RANS method show the effect of the higher solids loading at the center of the channel by the shifting of the maximum air velocity to a position that is closer to the wall.

Fig. 2 also depicts the normalized axial velocity of the carrier fluid, but now a polydisperse mixture of particles (mixture A) is carried. Mixture A is composed of equal parts (33.3%) of particles with diameters $d_2 = 0.50$ mm, $d_1 = 0.45$ mm and $d_3 = 0.55$ mm, that is there is a 10% deviation from the mean diameter of 0.5 mm and is the same as that examined by Tsuji et al. (1984). The data from the latter study are also shown in the Figure for comparison. When this Figure is compared to Fig. 1, it may be is observed that the polydispersity of the particulate mixture has a small but not significant effect on the axial velocity of the gas obtained from the two models.

Fig. 3 depicts, again, the carrier fluid axial velocity profile, with another solids mixture (mixture B) composed of equal parts (33.3%) of spheres with diameters $d_2 = 0.5$, $d_1 = 0.25$ and $d_3 = 0.75$ mm, that is there is a 50% deviation from the mean diameter. It is observed that, in this case, the results from the RANS method exhibit a maximum at the center of the channel. This is attributed to the higher dispersivity and collisions of the very small particles ($d_1 = 0.25$ mm) that constitute one third of the solids loading. It is also observed that the results from the RANS and the PDF methods are very close.

Fig. 4 depicts the solid phase velocity for mixture A, (equal parts of 0.50, 0.45 and 0.55 mm spherical particles) and also shows the experimental data obtained by Tsuji et al. (1984). It is observed that the results by RANS and PDF agree very well with the experimental data.

Since the lift force was not taken into consideration in the PDF model, we conducted a separate computation with the RANS method excluding the lift force, but still keeping all the other effects, such as gravity and particle collisions. The results are shown in Fig. 4a, which includes the normalized solids concentration and the normalized gas and solids velocities. It is observed that the gas and solids velocities obtained from the RANS model when the lift force is absent are significantly closer to those obtained

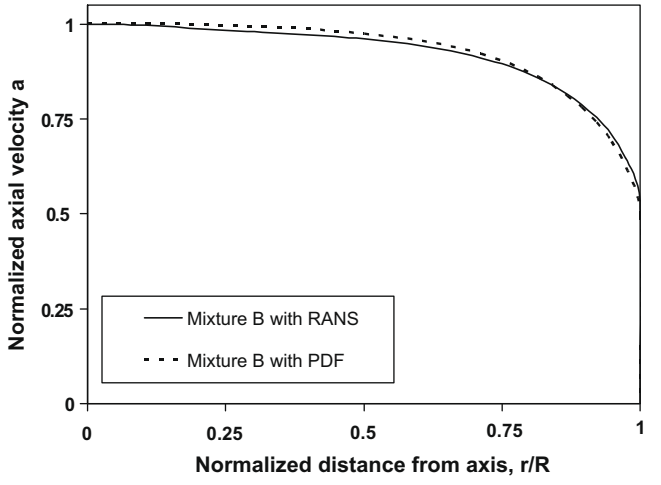

Fig. 3. Axial velocity profile of air with a solids mixture composed of equal parts of spheres with diameters 0.50, 0.25 and 0.75 mm.

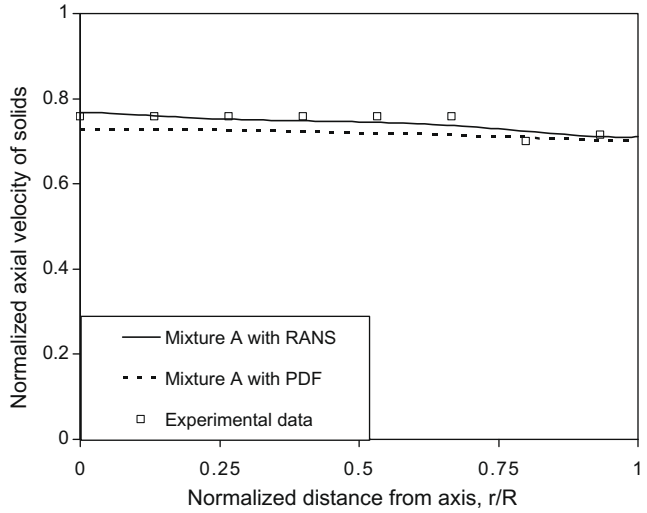

Fig. 4. Axial velocity profile of solids with a mixture composed of equal parts of spheres with diameters 0.50, 0.45 and 0.55 mm. The experimental data are from Tsuji et al. (1984).

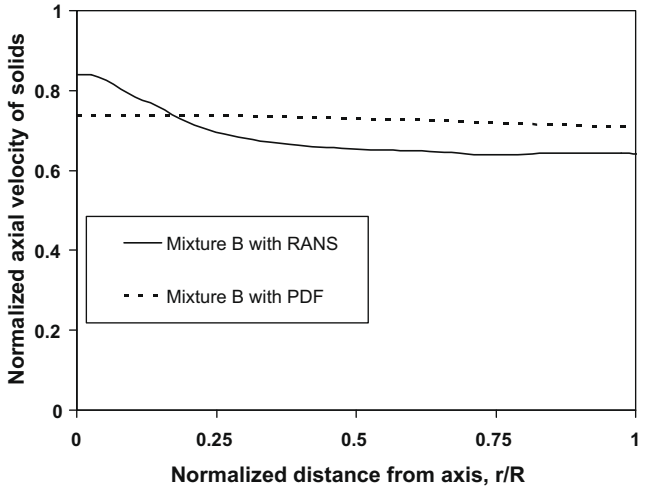

Fig. 5. Axial velocity profile of solids with a mixture composed of equal parts of spheres with diameters 0.50, 0.25 and 0.75 mm.

from the PDF method. Also, the almost solids concentration obtained from these computations is almost identical to that obtained from the PDF model. It is apparent from this figure that, while the absence of lift does not explain the differences observed in their entirety, it is the most important cause for the differences in the numerical data.

Fig. 5 also shows the solid phase velocity and corresponds to the results of Fig. 3 for the carrier fluid. Mixture B is composed of equal parts of spheres with diameters 0.5, 0.25 and 0.75 mm. It is observed that, as a result of the addition of the finer particles, the RANS results show a more pronounced peak at the center of the channel, while the PDF results are rather insensitive to this change of the solids composition and show an almost uniform velocity profile.

Fig. 6 depicts the normalized turbulent kinetic energy of air (turbulence intensity) when the channel carries solids corresponding to mixture A. It is observed that the results obtained from the two methods exhibit a sharp maximum close to the wall of the channel, but the numerical value of this maximum is significantly different. It is also observed that the results obtained by the RANS method are closer to the experimental data by Tsuji et al. (1984).

The profile of the average radial velocity of the solid particles for mixture A is shown in Fig. 7, where it is observed that the results emanating from the RANS model show a finite but very small velocity, while the PDF results indicate a vanishing radial velocity. This indicates that, in the RANS results, the solid particles' mixture re-arranges itself in the radial direction, most probably under the action/influence of the radial component of turbulence and the lift forces.

The concentration profile of the solids phase is shown in Fig. 8 for air carrying monodisperse solids of 0.50 mm diameters. It is obvious that the results obtained using the PDF method do not show the marked profile exhibited by the results of the RANS method. It is believed that this is due to the fact that lift forces are not taken into account in the PDF algorithm that was used for this study.

Fig. 9 depicts the results obtained by the two methods for air carrying the polydisperse mixture A, which is composed of equal

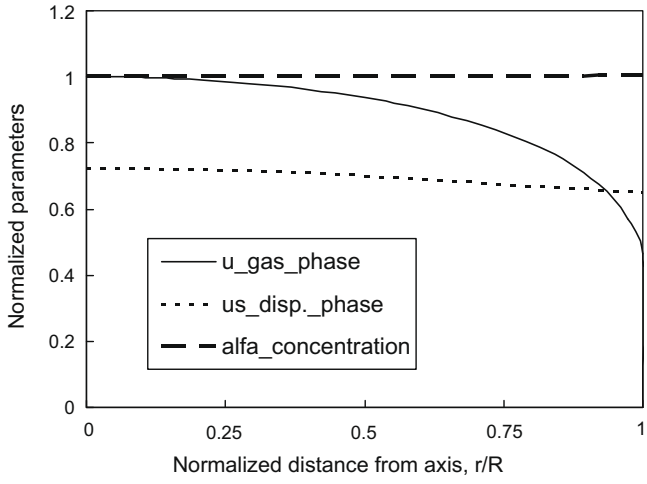

Fig. 4a. RANS computations excluding the lift force. Axial velocity profile of gas and solids and solids concentration with a mixture composed of equal parts of spheres with diameters 0.50, 0.45 and 0.55 mm.

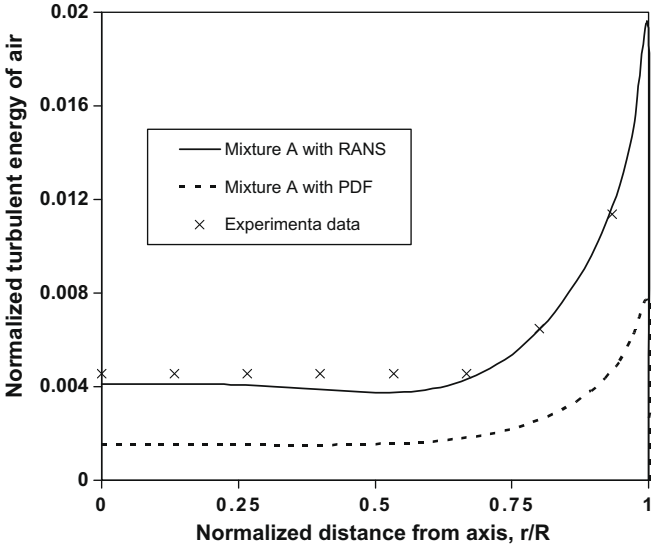

Fig. 6. Turbulent energy of the carrier fluid with a mixture composed of equal parts of spheres with diameters 0.50, 0.45 and 0.55 mm. The experimental data are from Tsuji et al. (1984).

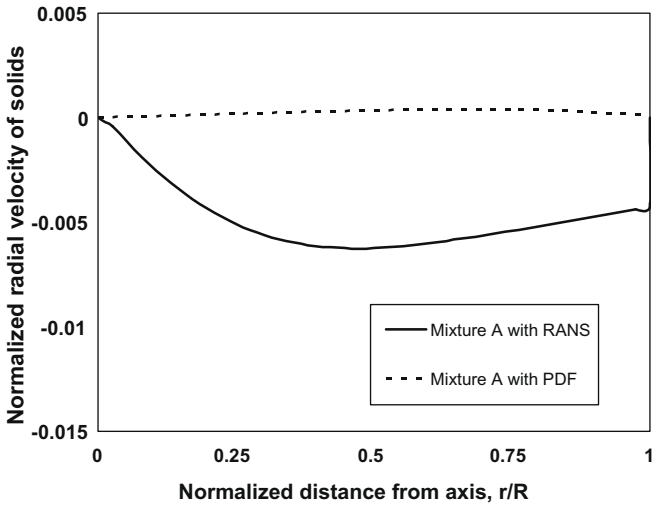

Fig. 7. Radial velocity profile of solids with a mixture composed of equal parts of spheres with diameters 0.50, 0.45 and 0.55 mm.

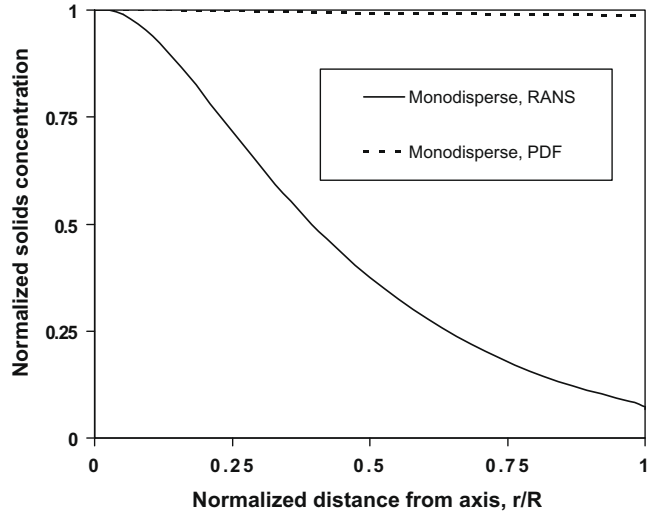

Fig. 8. Concentration profile of the solids phase with particles of 0.50 mm.

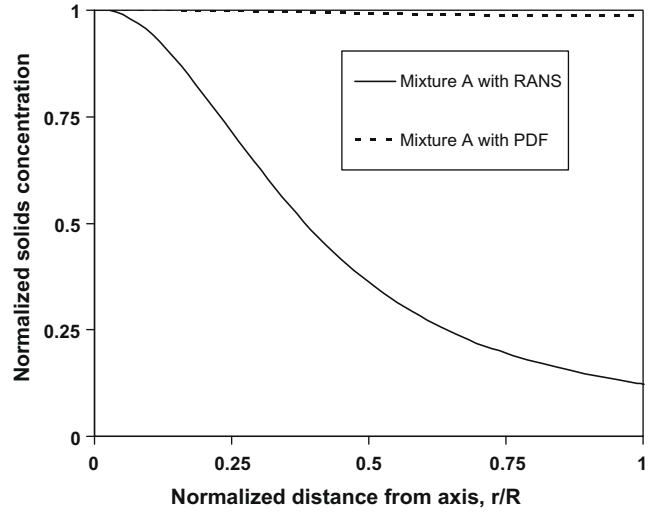

Fig. 9. Concentration profile of solids with a mixture composed of equal parts of spheres with diameters 0.50, 0.45 and 0.55 mm.

parts of spheres with 0.5, 0.45 and 0.55 mm diameters. Again, the most striking difference is the uniformity of the profile obtained by the PDF method, which is due to the absence of the action of the lift forces.

5. Conclusions

RANS and PDF are two methods that are widely used in the modeling of gas–solids flows, with each one having its own advantages and disadvantages. We have compared the results of the two methods in the case of an axisymmetric channel upward flow with inertial particles and a moderate loading of 3.4. The results showed that the two methods produce results for the axial velocity of the gas-phase that agree reasonably well, with the RANS method showing the shift in the maximum velocity. The results of the two methods for the velocity of the solids are very similar and are in good agreement with available experimental data. The results of both methods exhibit the pronounced maximum in the turbulent intensity of the carrier phase near the wall, although the numerical values of this maximum intensity differ significantly. Finally, the solids concentration profiles obtained by the PDF method show an almost uniform concentration, which is due to the absence of the action of lift forces on the solids. It is believed, that the addition of the lift forces in the PDF algorithms would have resulted in data obtained by the PDF and the RANS methods that are significantly similar.

Acknowledgements

This work was partly supported by Project SF0140070s08 (Estonia) and ETF Grant Project ETF7620. The authors are grateful for technical support of cluster computers of "Eesti Grid" and of the University of Texas at San Antonio.

References

Crowe, C.T., Gillandt, I., 1998. Turbulence modulation of fluid-particle flows – a basic approach. In: Third International Conference on Multiphase Flows, Lyon.
Crowe, C.T., Sommerfeld, M., Tsuji, Y., 1998. Multiphase Flows with Droplets and Particles. CRC Press LLC, Boca Raton, Florida.
Ding, J., Lyczkowski, R.W., Sha, W.T., Altobelli, S.A., Fukushima, E., 1993. Numerical analysis of liquid–solids suspension velocities and concentrations obtained by NMR imaging. Powder Technol. 77, 301–312.
Elghobashi, S., Abou-Arab, T.W., 1983. A two-equation turbulence model for two-phase flows. Phys. Fluids 26, 931–938.
Fevrier, P., Simonin, O., 2001. Statistical and continuum modeling of turbulent reactive particulate flows – Part II: application of a two-phase second-moment transport model for prediction of turbulent gas-particle flows. In: Buchlin M. (Ed.), von Karman Institute Lecture series. Brussels, Belgium.
Hussainov, M., Kartushinsky, A., Mulgi, A., Rudi, Ü., Tisler, S., 1996. Gas–solid flow with the slip velocity of particles in a horizontal channel. J. Aerosol Sci. 27, 41–59.
Kartushinsky, A., Michaelides, E.E., 2004. An analytical approach for the closure equations of gas–solid flows with inter-particle collisions. Int. J. Multiphase Flow 30, 159–180.
Matsumoto, S., Saito, S.J., 1970. Monte Carlo simulation of horizontal pneumatic conveying based on the rough wall model. Chem. Eng. Jpn. 3, 223–230.
Mei, R., 1992. An approximate expression for the shear lift force on a spherical particle at finite Reynolds number. Int. J. Multiphase Flow 18, 145–147.
Michaelides, E.E., 1984. A model for the flow of solid particles in gases. Int. J. Multiphase Flow 10, 61–75.
Michaelides, E.E., 2006. Particles, Bubbles and Drops – Their Motion, Heat and Mass Transfer, World Scientific Publishers, New Jersey.
Morioka, S., Nakajima, T., 1987. Modeling of gas and solid particles two-phase flow and application to fluidized bed. J. Theor. Appl. Mech. 6, 77–88.
Peric, M. Scheuerer, G., 1989. CAST – A finite volume method for predicting two-dimensional flow and heat transfer phenomena, GRS – Technische Notiz SRR – 89–01.
Pfeffer, R., Rosetti, S., Licklein, S., 1966. Analysis and correlation of heat transfer coefficient and heat transfer data for dilute gas–solid suspensions. NASA Report TND-3603.
Pourahmadi, F., Humphrey, J.A.C., 1983. Modeling solid–fluid turbulent flows with application to predicting arosive wear. Phys. Chem. Hydrodyn. 4, 191–219.

Reeks, M.W., 1991. On a kinetic equation for the transport of particles in turbulent flows. Phys. Fluids 3, 446–456.
Rubinow, S.I., Keller, J.B., 1961. The transverse force on a spinning sphere moving in a viscous fluid. J. Fluid Mech. 11, 447–459.
Shraiber, A.A., Yatsenko, V.P., Gavin, L.B., Naumov, V.A., 1990. Turbulent Flows in Gas Suspensions, Hemisphere Pub. Corp., New York.
Simonin, O., 2001. Statistical and continuum modeling of turbulent reactive particulate flows- Part I: theoretical derivation of dispersed phase Eulerian modeling from probability density function kinetic equation. In: Buchlin J.-M. (Ed.), von Karman Institute Lecture series. Brussels, Belgium.
Tsuji, Y., Morikawa, Y., Shiomi, H., 1984. LDV measurements of an air–solid two-phase flow in a vertical pipe. J. Fluid Mech. 139, 417–434.
Yarin, L.P., Hetsroni, G., 1994. Turbulence intensity in dilute two-phase flows. Parts I, II and III. Int. J. Multiphase Flow 20, 1–44.
Yuan, Z., Michaelides, E.E., 1992. Turbulence modulation in particulate flows – a theoretical approach. Int. J. Multiphase Flow 18, 779–791.
Wang, L.-P., Stock, D.E., 1993. Dispersion of heavy particles by turbulent motion. J. Atmos. Sci. 50, 1897–1913.
Zaichik, L.I., Vinberg, A.A., 1991. Modeling of particle dynamics and heat transfer in turbulent flows using equations for first and second moments of velocity and temperature fluctuations. In: Proceedings of the Eighth International Symposium on Turbulent Shear Flows, vol. 1, Munich, FRG, pp. 1021–1026.
Zaichik, L.I., Fede, P., Simonin, O., Alipchenkov, V.M., 2007. Comparison of two statistical approaches for modeling collision in bidisperse mixture of particles settling in homogeneous turbulent flows. Sixth ICMF-2007, July 9–13. Leipzig, Germany.